International Journal of Pharmaceutics 591 (2020) 119993

Contents lists available at ScienceDirect

International Journal of Pharmaceutics

journal homepage: www.elsevier.com/locate/ijpharm

Downregulation of *MDR 1* gene contributes to tyrosine kinase inhibitor induce apoptosis and reduction in tumor metastasis: A gravity to space investigation

Imran Tariq [a,b], Muhammad Yasir Ali [a,c], Harshavardhan Janga [d], Sajid Ali [a], Muhammad Umair Amin [a], Ghazala Ambreen [a], Uzma Ali [a], Shashank Reddy Pinnapireddy [a,e], Jens Schäfer [a], Leon N. Schulte [d], Udo Bakowsky [a,*]

[a] Department of Pharmaceutics and Biopharmaceutics, University of Marburg, Robert-Koch- Str. 4, 35037 Marburg, Germany
[b] Punjab University College of Pharmacy, University of the Punjab, Allama Iqbal Campus, 54000 Lahore, Pakistan
[c] Department of Pharmaceutics, Faculty of Pharmaceutical Sciences, GC University Faisalabad, Faisalabad, Pakistan
[d] Institute for Lung Research, Universities of Giessen and Marburg Lung Center, Philipps University Marburg, German Center for Lung Research (DZL), Hans-Meerwein-Str. 2, 35032 Marburg, Germany
[e] CSL Behring GmbH, Emil-von-Behring-Str. 76, 35041 Marburg, Germany

ARTICLE INFO

Keywords:
3D bioprinting
Apoptosis
Gene silencing
Imatinib mesylate
MDR
P-gp
PAMAM
Spheroids

ABSTRACT

P-glycoprotein (P-gp) associated multidrug resistance (MDR) represents a major failure in cancer treatment. The overexpression of P-gp is responsible for ATP-dependent efflux of drugs that decrease their intracellular accumulation. An effective downregulation of *MDR1* gene using small interfering RNA (siRNA) is one of the safe and effective tools to overcome the P-gp triggered MDR. Therefore, the development of an efficient and non-toxic carrier system for siRNA delivery is a fundamental challenge for effective cancer treatment. Polyamidoamine (PAMAM) dendrimer has been used for efficient delivery of siRNA (dendriplexes) to the tumor cells but the associated toxicity problems render its use in biological applications. A non-covalent lipid modification (lipodendriplexes) is supposed to offer a promising strategy to overcome the demerits linked to the naked dendriplexes system. In the current study, we deliver siRNA, designed against *MDR1* gene (si-*MDR1*), in colorectal carcinoma cells (Caco-2), having overexpression of P-gp, to check the role of *MDR1* gene in tumor progression and multidrug resistance using two dimensional (2D) and three dimensional (3D) environment. Imatinib mesylate (IM), a P-gp substrate, was used as model drug. Our results revealed that the effective knockdown by lipodendriplexes system can significantly reduce the tumor cell migration in 2D ($p < 0.001$) and 3D ($p < 0.001$) cell cultures as compared to unmodified dendriplexes and si-Control groups. It was also observed that lipodendriplexes aided downregulation of *MDR1* gene effectively, re-sensitized the Caco-2 cells for IM uptake and showed a significantly ($p < 0.001$) higher apoptosis. Our findings imply that our lipodendriplexes system has a great potential for siRNA delivery, however, further *in vivo* application using a suitable targeted system can play a major role for better cancer therapeutics.

1. Introduction

Multidrug resistance (MDR) is a phenomenon to develop a cross-resistance in tumor cells accompanied by a decreased or altered intracellular accumulation of chemotherapeutic drugs. In many cases, MDR of chemotherapeutic drugs is highly associated with the overexpression of P-glycoproteins (P-gp), encoded by the *MDR1* gene. The P-gp are overexpressed on the plasma membrane of the cancerous cells where it can trigger the ATP driven efflux of most of the anti-tumor drugs, lead to a reduced accumulation of the drug in the targeted tumor cells and subsequent failure of the chemotherapy (Tsuruo et al., 2003; Risnayanti et al., 2018). P-gp associated MDR can be tackled by the use of many P-gp inhibitors (Dantzig et al., 2003) or substrates (Ni et al., 2011), however, the side effects, off-targeting to tissues, and interaction with many chemotherapeutic drugs limit their use for clinical purpose. Therefore, a safe alternative tool to downregulate the expression of P-gp,

* Corresponding author.
E-mail address: ubakowsky@aol.com (U. Bakowsky).

https://doi.org/10.1016/j.ijpharm.2020.119993
Received 6 July 2020; Received in revised form 7 October 2020; Accepted 14 October 2020
Available online 18 October 2020

to silence the *MDR1* gene, can be a double-stranded small interfering RNA (siRNA) (Essex et al., 2014). In gene silencing mechanism, siRNA enters the cells by the endocytosis process and after crossing the endosomal membrane it gets loaded into RNA induced silencing complex (RISC) for the selective binding with the complementary mRNAs, to induce a catalytic degradation (silencing) of the targeted gene (Gilleron et al., 2013).

On the other hand, P-gp are also present in the normal healthy tissue of the body and has a crucial role to perform different vital functions. Therefore, a carefully designed siRNA is the prerequisite to avoid off-targeting to the normal cells (MacDiarmid et al., 2009; Jiang et al., 2010).

Polyamidoamine (PAMAM) dendrimer with ethylenediamine core has been used for an efficient siRNA delivery (Zhou et al., 2006). The primary amine groups of the PAMAM mostly participate in the binding with the siRNA to make a stable nano-complex (dendriplexes) for subsequent transfection of the complexes into the cells, while the tertiary amino groups act as proton sponge in the endosomal environment to facilitate the release of siRNA into the cytoplasm (Dutta et al., 2006). It has also been reported that PAMAM dendrimer having terminal amino groups significantly possesses hemolytic toxicity and cytotoxicity (Jain et al., 2010). Therefore, a non-covalent lipid modification of dendriplexes can reduce their cytotoxicity and considerably enhance the cellular uptake to targeted cancer cells and lead to an efficient gene knockdown (Dutta et al., 2010).

Imatinib mesylate (IM), a BCR-ABL tyrosine kinase inhibitor (Druker et al., 2001) has been approved by FDA for the treatment of chronic myeloid leukemia (CML) (Iqbal and Iqbal, 2014). Recently, it has also been investigated against other tumors like gastrointestinal stromal tumors (GIST) (Balachandran et al., 2011) and colon carcinoma (Graber-Maier et al., 2010). Imatinib mesylate is also a substrate of P-gp, therefore the overexpression of P-gp and BCR-ABL protein in a cell line can elicit resistance against imatinib (Mahon et al., 2003; Galimberti et al., 2005). However, a sequential treatment to deliver si-*MDR1* (MDR modulation) and imatinib mesylate (apoptotic inducer) can be considered a promising strategy against MDR cancer therapy (Biswas et al., 2013; Sarisozen et al., 2017; Saw et al., 2017). The downregulation of P-gp by si-*MDR1* can re-sensitize the tumor resistant cell and contributes to the apoptotic induction of IM by increasing its intracellular accumulation (Stromskaya et al., 2008; Negi et al., 2015).

Traditionally, a sequential effect of gene silencing followed by chemotherapeutic treatment has been evaluated in two-dimensionally (2D) cell culture but these simulations can sometimes deprive of clinical outcome, due to their poor predictability for the normal physiological conditions. Therefore, to portray an *in vivo* like condition, three dimensional (3D) cell culture models are supposed to be a better reflection of the original tumor, by their ability to generate extracellular matrix (ECM) among the cell cluster in a hypoxic environment (Terashima et al., 2016).

In our previous work, we have developed a state of the art optimized lipodendriplexes system (Tariq et al., 2019), having negligible cytotoxicity with enhanced gene transfection efficiency. Therefore, using our safe and efficient nanocarrier system, the aim of the current study was to investigate its efficacy for RNA interference, against *MDR1* gene using Caco-2 cell line (having overexpression of P-gp). The formulations were initially characterized using dynamic light scattering, laser Doppler anemometry and atomic force microscopy. *In vitro* toxicity studies including ROS, MTT, lysosomal disruption and DNA damage assays were performed in the Caco-2 cell line to evaluate the biocompatibility of the complexes. Afterward, the *MDR1* silencing effect was investigated in 2D and 3D cell culture, to check the contribution of *MDR1* gene in tumor progression and MDR.

From the current study, we were expecting to **(i)** increased intracellular uptake of si-*MDR1* by endocytosis mechanism, **(ii)** down-regulation of P-gp expression after knockdown of *MDR1* gene, **(iii)** inhibition in *MDR1* regulated cell migration, **(iv)** reversal of MDR and **(v)** subsequently enhanced apoptosis by imatinib mesylate.

2. Materials and methods

2.1. Materials

1,2-dipalmitoylphosphatidylcholine (DPPC) lipid was a kind gift from Lipoid AG (Steinhausen, Switzerland). PAMAM dendrimer, ethylenediamine core, generation 5 solution (5%) in methanol, cholesterol (CH), 4-(2-hydroxyethyl)-1-piperazineethanesulfonic acid (HEPES), 2,7-dichlorofluorescin diacetate (H_2DCFDA), 4′,6-diamidino-2-phenylindole (DAPI) and 3-(4,5-dimethylthiazolyl-2)-2,5-diphenyltetrazolium bromide (MTT) were obtained from Sigma Aldrich Chemie GmbH (Taufkirchen, Germany). Dimethyl sulfoxide (DMSO) was purchased from Carl Roth GmbH & Co. Kg (Karlsruhe, Germany). SYBR® Safe DNA dye, Lyso Tracker® red DND-99, High Capacity cDNA Reverse Transcription Kit, PowerUp™ SYBR™ Green Master Mix, Pierce protein BCA assay kit and heparin sodium salt, from porcine intestinal mucosa were purchased from Thermo Fischer Scientific (Dreieich, Germany). RNeasy mini kit was purchased from Qiagen (Hilden, Germany). 96-well Bio assay™ kit was a gift sample from Greiner Bio-One GmbH (Frickenhausen, Germany). Dulbecco's modified Eagle's minimum essential medium (DMEM), fetal bovine serum (FBS) and non-essential amino acid (NEA) were purchased from Capricon Scientific (Ebsdorfergrund, Germany). Purified water from PURELAB flex II dispenser (ELGA LabWater, High Wycombe, UK) was used for all the experiments. All other reagents used in experiments were of analytical grade.

2.2. Oligonucleotides

siRNA duplexes against *MDR1* gene (si-*MDR1*) (sense 5′ GAU GAU GUC UCC AAG AUU AdTdT 3′; sense 5′ GUC ACU GCC UAA UAA AUA UdTdT 3′; sense 5′ GAU CGC UAC UGA AGC AAU AdTdT 3′), a non-targeting non-specific scrambled siRNA (si-Control) to have no silencing effects on rat, mouse and human genes and gene-specific primers (forward 5′ TTCAGGTGGCTCTGGATAAG 3′ and reverse 5′ TCAGCATTACGAACTGTAGACA 3′) were purchased from Eurogentec (Seraing, Belgium).

2.3. Cell line and culturing

Homosapiens colorectal adenocarcinoma (Caco-2) cell line was a kind gift from the Institute for Lung Research, University of Marburg, Germany. Caco-2 cell line was cultured in DMEM (containing 10% FBS supplemented with 10% NEA) at 37 °C and 5% CO_2 under humid conditions). All cells were cultivated as monolayers and passaged upon reaching 80% confluency.

2.4. Preparation of lipodendriplexes

Lipodendriplexes were prepared in the same manner described previously (Tariq et al., 2019). Briefly, PAMAM dendrimer solution was mixed with equal volumes of si-*MDR1* solution using N/P ratio 12 (the ratio of terminal amino groups of PAMAM to the phosphate groups of nucleic acid) by vigorous pipetting, followed by incubation at room temperature for 30 min. The resulting dendriplexes were then mixed with a fine dispersion of liposomes (DPPC: CH; 85:15) at the liposome to PAMAM dendrimer mass ratio of 0.5 and incubated at room temperature for 1 h.

2.5. Physicochemical characterization

2.5.1. Dynamic light scattering and laser Doppler anemometry

The hydrodynamic diameter and zeta potential of the lipodendriplexes were determined by dynamic light scattering (DLS) and laser Doppler anemometry (LDA) techniques by Zetasizer Nano ZS

(Malvern Instruments, Malvern, UK), using a clear disposable folded capillary cell (DTS1060, Malvern Instruments). Prior to measurements, the samples were diluted (1:100 ratio) with purified water. The results were calculated from the measurements of three independent formulations (mean ± standard deviation).

2.5.2. Atomic force microscopy (AFM)

The surface morphology of the lipodendriplexes was characterized by atomic force microscopy (AFM) on NanoWizard® 3 NanoScience (JPK Instruments, Berlin, Germany). Briefly, 20 µl of the sample was placed on the surface of the silica wafer and was allowed to adsorb on it for 10 min. AFM images were acquired at room temperature using intermittent contact mode, at a resonance frequency of 160 kHz, by commercially available cantilever tips (NSC14 AlBS, Micromash Europe, Wetzlar, Germany). The results of images were processed using JPK data processing software v 6.1.62.

2.6. Determination of reactive oxygen species (ROS)

For reactive oxygen species (ROS) generation assay, Caco-2 cells were seeded at the seeding density of 25,000 cells per well in 96-well microtiter plates and were incubated overnight. For the measurement of ROS production, cellular ROS protocol by Abcam (Cambridge, UK) was used with slight modifications. Briefly, 100 µl of 25 µM cell-permeant reagent 2,7-dichlorofluorescein diacetate (H_2DCFDA) was loaded to the cells for 1 hour at 37 °C. The cells were then washed thrice with PBS and incubated with the complexes for 1 h at a final siRNA concentration of 36 nM using 50 µM tert-Butyl hydroperoxide (TBHP) as a positive control. The cells were washed again with PBS and fluorescence of dichlorofluorescein (DCF) was detected using excitation and emission wavelengths of 485 nm and 520 nm, respectively (FLUOstar Optima), to quantify the levels of ROS production. The intracellular fluorescence visualization was monitored by a microscope (CKX-53 Olympus, USA), equipped with GFP fluorescence detection filters (ex.505 nm - em.530 nm) (Duse et al., 2018; Mahmoud et al., 2018).

2.7. In vitro cell viability assay

For *in vitro* cell viability assay, Caco-2 cells were seeded at a seeding density of 10,000 cells per well in 96-well microtiter plates and were incubated overnight. After incubation, the cells were incubated with the complexes at the final siRNA concentration of 36 nM for 4 h, using 1% Triton^{TM}X-100 as a positive control. Afterward, an additional medium was added and incubated for a further 20 h. The medium of the plates was replaced by MTT reagent and were incubated for further 4 h. After the incubation, DMSO was added to dissolve the formazan crystals formed by the metabolism of the MTT dye by viable cells. The plates were then rotated on a shaking incubator (KS4000 IC, IKA Werke, Staufen, Germany) for 15 min. The absorbance of formazan was measured at 570 nm (FLUOstar Optima). The cell viability of the cells was expressed as a percentage of viability of the treated cells to untreated cells.

2.8. Lysosomal disruption and actin polymerization

Caco-2 cells were seeded at the seeding density of 90,000 cells per well in a 12-well cell culture plates containing coverslips (15 mm diameter). After 24 h incubation, the old culture medium of the cells was replaced with the fresh medium and incubated with the complexes at the final siRNA concentration of 36 nM. Cells were incubated with the complexes for 4 h followed by incubation with 100 nM of Lyso Tracker® red DND-99 for 30 min at 37 °C to stain the lysosome. The cells were then washed with PBS containing Ca^{2+} and Mg^{2+} before fixing with 4% formaldehyde solution (Guo et al., 2018). Thereafter, cell nuclei were stained with DAPI, followed by actin cytoskeleton staining with Phalloidin-FITC. The coverslip was placed on a clear glass slide and sealed with fluorescence-free glycerol-based mounting medium (FluorSave™, Calbiochem, San Diego, USA) before being analysed under a fluorescence microscope (CKX-53 Olympus, USA).

2.9. DNA damage assay

DNA damage was analysed by the comet assay (Ali et al., 2020). Briefly, Caco-2 cells were seeded at the seeding density of 90,000 cells per well in a 12-well cell culture plate and incubated overnight. After incubation, the old culture medium was replaced with the fresh medium and incubated with the complexes at the final siRNA concentration of 36 nM for 4 h. After incubation, additional 1 ml of medium was added to the wells and incubated up to 48 h. The cells were washed thrice with ice-cold PBS containing Ca^{2+} and Mg^{2+}. The cells were then trypsinized and suspended (8000 cells in 25 µl of PBS) in 75 µl of low melting agarose 1% (LMA) and placed on pre-coated microscopic slides (Super frost microscopic slides were coated with 1% normal melting point agarose (NMA) and the lower surface was wiped before the settling of gel). The gel was covered with glass coverslips and allowed to set on an ice block. The coverslips were carefully removed and the settled gel was sandwiched by an additional layer of LMA. The slides were then gently placed in ice-cold lysis buffer (2.5 M NaCl, 100 mM EDTA, 10 mM Tris, 1% Triton™ X-100; pH 10) and incubated overnight at 4 °C under dark condition. Afterward, the microscopic slides were placed in alkaline electrophoresis solution (300 mM NaOH, 1 mM EDTA; pH > 13) for 20 min to start the DNA unwinding process. Gel electrophoresis was performed under refrigerating conditions at 25 V and 250 mA for 30 min. The level of the electrophoresis solution should not be more than 5 mm above the gel. Subsequently, the slides were removed from the electrophoresis chamber and rinsed with ice-cold neutralizing buffer (400 mM Tris buffer; pH 7.5) for 5 min to remove the alkaline traces. The slides were dried and fixed with 70% ethanol for 15 min. Thereafter, slides were stained with SYBR® safe DNA gel stain for 20 min in dark condition. The cells were analysed by scoring 50 comets per slide using a microscope (CKX-53 Olympus, USA), equipped with GFP fluorescence detection filters (ex.505 nm - em.530 nm). The comets were analysed using Comet IV software (Instem, Staffordshire, UK).

2.10. RNA interference experiments

2.10.1. MDR1 silencing

The knockdown of *MDR1* gene experiment was conducted in the *MDR1* gene expressing Caco-2 cell line. Cells were seeded in 6-well cell culture plates (Sarstedt AG & Co. KG, Nümbrecht, Germany) at the seeding density of 1,00,0000 cells per well. After overnight incubation, the cells were transfected with complexes at the final si-*MDR1* concentration of 36 nM and incubated for 48 h. After incubation, the cells were washed with PBS followed by the trypsinization of the cells. The cells were collected and resuspended in PBS and subjected to RNA isolation.

2.10.2. RNA isolation, reverse transcription and real-time quantitative PCR

Total RNA was isolated using the RNeasy Mini Kit, according to the manufacturer's instruction. After measuring the amount of isolated RNA, cDNA was synthesized using a High Capacity cDNA Reverse Transcription Kit, according to the manufacturer's protocol. A 20 µl reactions mixture was subjected for a thermal cycler program as follows, 25 °C for 10 min, 37 °C for 120 min, 85 °C for 5 min and then held at 4 °C. The quantitative real-time PCR assay was performed with Quant studio 3 RT-PCR System (Applied Biosystems, Foster City, CA) using PowerUp™ SYBR® Green Master Mix, according to the manufacturer's instructions. A 10 µl of the reaction mixture was used for RT-qPCR containing 15 ng of cDNA and 0.4 µl of 10 mM gene-specific primers. GPDH (housekeeper gene) was used as a positive control and Ct values were used to calculate the relative mRNA expression level.

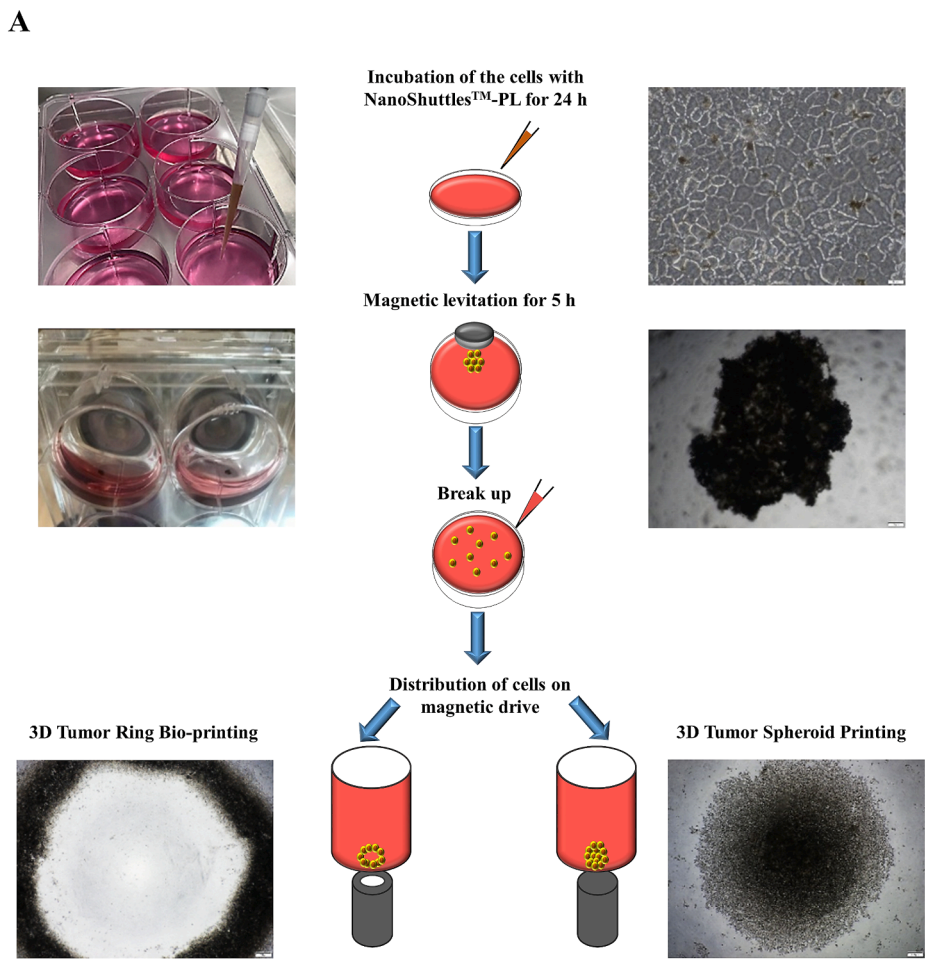

Fig. 1. (A) Schematic representation of 3D tumor spheroid and 3D tumor ring bioprinting formation by magnetic levitation method. (B) Steps involved in spheroid formation: (a) Addition of Nano-Shuttles™-PL in the cells. (b) Trypsinization and washing of cells. (c) Addition of cells in 6-well ultra-low attachments plate and placement of the lid. (d) Placement of levitating drive (e) Incubation for 5 h to generate the ECM among the cells. (f) Formation of cells aggregates and break down. (g) Placement of 96-well ultra-low attachment plate on a spheroid magnetic drive. (h) Addition of cells under the influence of the magnetic field. (i) Incubate the plate for 15 min to print spheroids.

2.10.3. Wound healing assay

Caco-2 cells were seeded at the seeding density of 1,00,0000 cells per well in a 6-well cell culture plates. After overnight incubation, the cells were transfected with complexes at the final si-*MDR1* concentration of 36 nM and incubated for 48 h. After 48 h of transfection period, the cells were trypsinized and washed with culture medium. Thereafter, 25,000 cells with a seeding volume of 70 µl were transferred into each chamber of culture insert of µ-Dish (Ibidi, Martius, Germany) and incubated overnight for their confluency. After incubation, culture inserts were removed and an additional medium (3 ml) was added in µ-Dish. Scratch closure was photographed to investigate the wound recovery at different time points (0, 16, 24, 48 h), using a microscope (CKX-53 Olympus, USA). The scratch closure area was calculated according to the gap filled by migrated cells in comparison to the scratch area at 0 h. Image J analysis software was used to calculate scratch closure.

2.10.4. Transwell migration assay

Caco-2 cells were grown in 6-well cell culture plates at a seeding density of 1,00,0000 cells per well. The cells were transfected with complexes at the final si-*MDR1* concentration of 36 nM and incubated for 48 h. After 48 h of transfection period, the cells were trypsinized and washed with a serum-free culture medium. Thereafter, 2,50,000 cells

with a seeding volume of 200 µl were transferred to the upper chamber of transwell insert (8 µm pore size, PET membrane; Corning, New York, USA). A 500 µl of culture medium with 20% FBS was added to the lower chamber and incubated the plate for 48 h. After incubation, the old medium was aspirated from the upper chamber of the insert and unmigrated cells were removed by the help of a wet cotton swab. The migrated cells attached to the lower part of the chamber were fixed with 70% ethanol and stained with 0.1% crystal violet dye. The cell migration was observed in five randomly selected stained area under a bright field microscope and analysed using Wimasis image analysis software.

2.10.5. Plate colony formation assay

Caco-2 cells were grown in 6-well cell culture plates at a seeding density of 1,00,0000 cells per well. The cells were transfected with complexes at the final si-*MDR1* concentration of 36 nM and incubated for 48 h. After 48 h of transfection period, the cells were trypsinized and resuspended in the new medium. Thereafter, 1000 cells were transferred into a well of 6-well cell culture plate and allowed to grow for 14 days. The cells were then fixed with 70% ethanol followed by washing with PBS. The cells were then stained with 0.1% crystal violet dye to detect the formation of colonies in the wells. The colony containing more than 50 cells was counted manually.

2.11. Formation of 3D tumor spheroids and 3D ring bioprinting

In two-dimensional (2D) cell culture assays, the cell vasculatures are not in direct contact with the biochemical components of the media. On the other hand, it is also difficult to regulate the extracellular matrix (ECM) for the diffusion of extracellular compounds in a 2D environment. To overcome these challenges, 3D magnetic bioprinting can play a novel role to pattern a 3D cell culture structure by magnetizing the cells with biocompatible magnetic nanoparticles i.e Nano3D Biosciences Nano-Shuttles™-PL (Greiner Bio-One GmbH, Frickenhausen, Germany). The NanoShuttles™-PL assembly consists of gold nanoparticles, iron oxide and poly-L-lysine, a biopolymer with a cell-adhesive peptide sequence. It performs the dual function to electrostatically bind to the cells and to cross-link with the nanoparticles (de Cássia Antonino et al., 2019). The binding of the nanoparticles with the cells generates the magnetic properties in the cell which can be influenced by the external application of a magnetic field. The process of magnetic levitation initiates the cell aggregation and generates the ECM among the cells. Afterward, the induction of the magnetic field rapidly patterns the cells into a spheroidal or ring shape (Fig. 1A&B). After the removal of the magnetic field, the cells tried to proliferate or migrate through ECM (Timm et al., 2013; Tseng et al., 2016).

2.11.1. 3D tumor spheroids cell migration

3D tumor spheroids were prepared by the magnetic levitation method using the 96-well Bio assay™ kit (Greiner Bio-One GmbH, Frickenhausen, Germany). Caco-2 cells were seeded in a 6-well cell culture plate at the seeding density of 1,00,0000 cells per well. After overnight growth, the cells were transfected with complexes at the si-*MDR1* concentration of 36 nM and incubated for 48 h. Afterward, the cells were incubated overnight with Nano3D Biosciences Nano-Shuttle™-PL (8 µl/cm^2 of cell culture area) to crosslink the nanoparticles with the cells. On the following day, the cells were washed, trypsinized and resuspended in the media. A 2 ml of cell suspension was then distributed in the 6-well ultra-low attachment plate (Greiner Bio-One GmbH, Frickenhausen, Germany) at the cell density of 2,50,000 cells per ml. The plates were then covered with the lid and the levitating drive was placed at the top of the lid. The plates were then rotated 3–4 times and observed under the microscope to check the initiation of the levitating process. The plate was then incubated for 5 h to generate the extracellular matrix (ECM) among the levitating cells. The levitating cells were then broken by pipetting action. Afterward, a 96-well ultra-low attachment plate (Greiner Bio-One GmbH, Frickenhausen, Germany) was placed on the magnetic spheroid drive and broken cells were distributed at the cell density of 50,000 cells per well. The cells were then allowed to print on the magnetic spheroid drive for 15 min to obtain a loose connected spheroidal structure. The magnetic spheroid drive was then removed from the bottom and the plate was incubated overnight to grow the tumor spheroid. The migration of cells through the ECM was then recorded for 48 h and the percentage (%) of cell migration was calculated according to the following formula:

$$\text{Cell migration } (\%) = \frac{\text{Area covered by migrating cells } (\mu\text{m})}{\text{Total area covered by bioprinted region } (\mu\text{m})} \times 100 \quad (1)$$

2.11.2. Cytoskeleton staining of spheroids

Spheroid formation was done in the same manner mentioned above. After the 48 h of incubation, the spheroids were washed with PBS containing Ca^{2+} and Mg^{2+} and fixed with 4% formaldehyde solution for 1 h. The spheroids were then washed twice with PBS and counterstained with DAPI followed by Phalloidin-FITC for nuclei and cytoskeleton visualization, respectively. For every step, the spheroids were anchored by a magnetic spheroid drive to maintain their structural integrity. The magnetic spheroids were then carefully pulled out using a Magpen (Greiner Bio-One GmbH, Frickenhausen, Germany) and placed on a clear glass slide under the influence of the magnetic field. A coverslip was then placed over the spheroids and sealed with a fluorescence-free glycerol-based mounting medium. The spheroids were then analysed under a microscope (CKX-53 Olympus, USA), equipped with fluorescence filters.

2.11.3. 3D tumor ring closure assay

For 3D ring bioprinting, the levitation of the cells was performed in the same manner discussed above. The levitating cells were then broken by pipetting action. Afterward, a 96-well ultra-low attachment plate was placed on the magnetic ring drive and broken cells were distributed at the cell density of 100,000 cells per well. The cells were then allowed to print on a magnetic ring drive for 15 min to obtain a loosely connected ring structure. The magnetic ring drive was then removed from the bottom and plates were incubated overnight to grow the tumor ring. The ring closure area was recorded for 48 h and compared with the si-Control. The percentage (%) of ring closure area was determined using the following formula:

$$\text{Ring closure area } (\%) = \frac{\text{Inner diameter } (\mu\text{m}) \text{ of ring after specified time interval}}{\text{Initial inner diameter } (\mu\text{m}) \text{ of the ring}} \times 100 \quad (2)$$

2.12. Apoptosis assay by flow cytometry

Cells apoptosis was investigated, according to the sequential treatment protocol, by flow cytometry (FACS) technique. Briefly, 90,000 Caco-2 cells per well were seeded overnight in 12-well cell culture plates. The cells were transfected with complexes at the final si-*MDR1* concentration of 36 nM and incubated for 48 h. After incubation, the

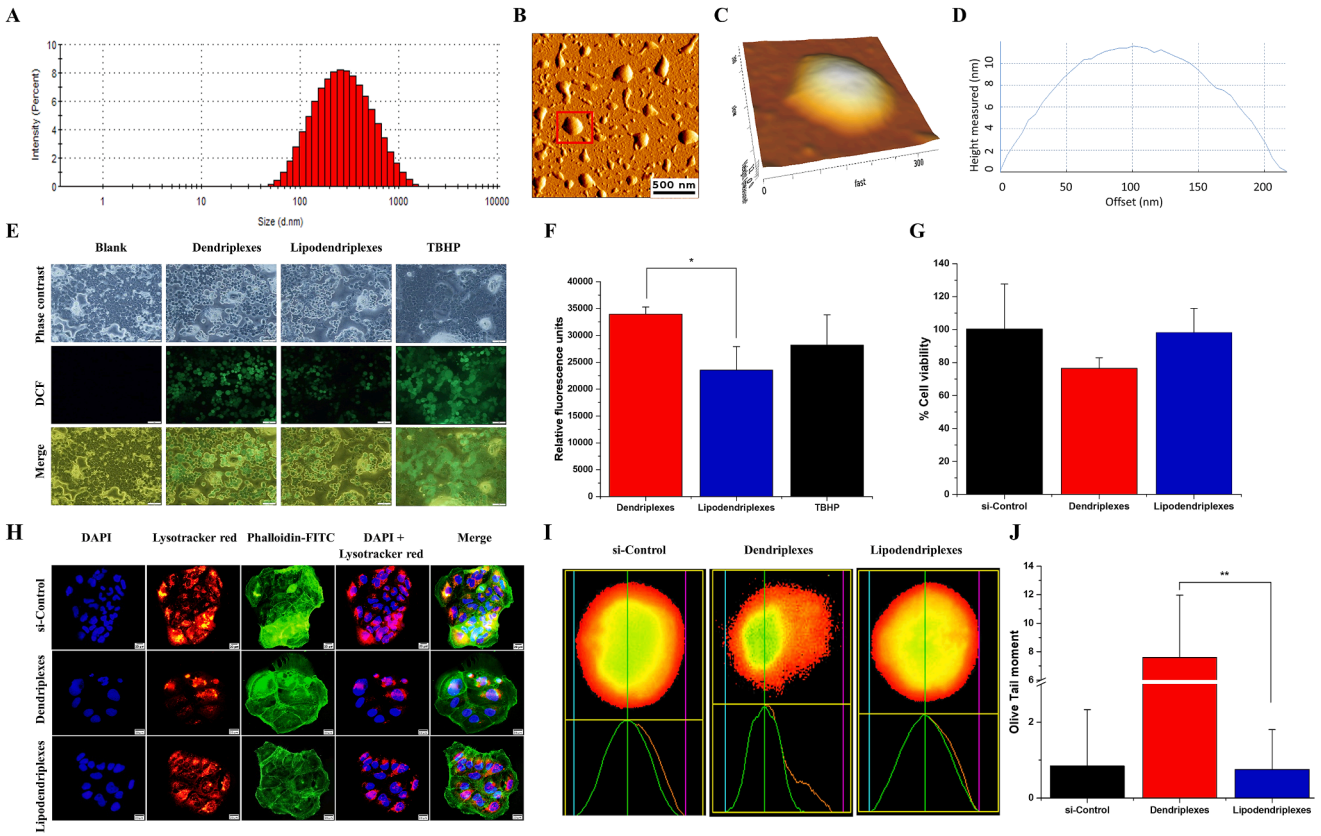

Fig. 2. (A) Size analysis of DPPC: CH-PAMAM lipodendriplexes. (B) AFM intermittent contact mode image of DPPC: CH-PAMAM lipodendriplexes using NSC14 AlBS cantilever; lock-in amplitude image of lipodendriplexes (scale bar represents as 500 nm). (C) 3D height representative view of the single lipodendriplex. (D) Cross-sectional height measured view of a single lipodendriplex showing a step height of 4 nm indicating a lipid bilayer. (E&F) Fluorescence micrograph and relative fluorescence units of intracellular ROS generation in Caco-2 cell lines, respectively after the addition of optimized complexes using TBHP as control. Higher DCF (green fluorescence) was produced from H_2DCFDA after the addition of dendriplexes to the cells in comparison to lipodendriplexes. Blank represents cells without any treatment. (G) *In vitro* cell viability studies. (H) Lysosomal disruption and actin polymerization assay; DAPI (blue) corresponds to the nuclei staining while Lysotracker red (red) represents lysosomal staining. Phalloidin FITC (green) representing the cytoskeleton staining to monitor actin polymerization. (I&J) DNA damage assay; olive tail moment representing the extent of DNA damage of optimized dendriplexes and DPPC: CH-PAMAM lipodendriplexes (N/P ratio 12) in Caco-2 cell line. Significantly higher olive tail moment was observed in the case of dendriplexes treated cells. Cells treated with non-specific scrambled siRNA considered as si-Control. Values are represented as mean ± S.D (n = 3) and statistical significances are indicated as *$p < 0.05$, **$p < 0.01$. Scale bar represents 20 μm. (For interpretation of the references to color in this figure legend, the reader is referred to the web version of this article.)

media was replaced by IM (75 μM) and incubated for further 24 h. The controlled cells were incubated without any addition of the drug. Afterward, the cells were collected, washed with cold PBS and resuspended in 1x binding buffer. A 50 μl of binding buffer supplemented with 1 μl (10 μg/ml) of APC Annexin V were gently mixed with an equal volume of cell suspension and incubated at room temperature for 15 min under dark condition. Afterward, 300 μl of binding buffer containing 0.4 μl (5 mg/ml) of propidium iodide (PI) was added and placed on ice for 5 min before analyse by flow cytometer (Guava®easyCyte™, Millipore Sigma, USA). The data was processed by Flowjo 10 software.

2.13. Apoptosis determination in spheroids by live dead viability assay

Tumor spheroids were formed in the manner discussed above. After the 24 h of spheroids formation, the media was replaced by IM (75 μM) and incubated for 24 h. The controlled spheroids were incubated without any addition of the drug. The spheroids were then washed with PBS before staining with a solution containing 3 μM syto 9 and 7.5 μM PI for live dead viability assay, using Live/Dead viability kit (Invitrogen™, Oregon, USA). The spheroids were then again washed with PBS and analysed under a microscope (CKX-53 Olympus, USA) equipped with fluorescence filters.

2.14. Cell cycle analysis by flow cytometry

For cell cycle analysis, briefly, 1,00,0000 Caco-2 cells per well were seeded overnight in 6-well cell culture plates. The cells were transfected with complexes at the si-*MDR1* concentration of 36 nM and incubated for 48 h. After incubation, the media were replaced by IM (75 μM) and further incubated for further 24 h. The controlled cells were incubated, without any addition of the drug. Afterward, the cells were trypsinized and washed with ice-cold PBS. The cells were then fixed by a dropwise addition of 70% ice-cold ethanol and stored at −20 °C for at least one hour. At the time of analysis, the cells pellet was washed twice with ice-cold PBS and suspended in 1 ml of PI/0.1% Triton™ X-100 staining solution (PI 20 μg and RNase 50 μg in 1 ml of 0.1% Triton™ X-100 solution). Keep the cell suspension in the dark condition at room temperature for 30 min. Just before the analysis, the cell suspension was vortexed and filtered using a polystyrene round-bottom tube equipped with a cell strainer cap. The cell suspension was poured in the cap and centrifuged for a short period. The cell cycle distribution was then analysed using a PE-A channel with a flow cytometer (BD Biosciences LSR II FACS, San Francisco, USA). A minimum of 20,000 events was measured per sample and data was analysed using ModFit LT V 5.0 software (using a special updated file for Sub-G1 phase calculation).

2.15. Statistical analysis

All experiments were performed in triplicates and the values are mentioned as a mean ± standard deviation. One-way Anova was performed to identify statistically significant differences using IBM SPSS software (Ver. 22). Dunnett's test was used for multi-comparison between the results and control, whereas multi-comparison among the different groups was made using Tukey's test. Statistical difference of P values more than 0.05 considered insignificant. *$p < 0.05$, **$p < 0.01$, ***$p < 0.001$.

3. Results and discussion

3.1. In vitro physicochemical characterization

In our previous work, optimized lipodendriplexes of N/P ratio 12 showed the highest gene transfection efficiency (Tariq et al., 2019). Therefore, this optimized non-viral nanocarrier was carried forward for gene silencing experiments (Dutta et al., 2006). In DLS and LDA analysis of lipodendriplexes, the average size and zeta potential were 213.1 ± 13.8 nm (Fig. 2 A) and 10.8 ± 1.6 mV (PDI = 0.2), respectively. The AFM findings showed a spherical morphology of the lipodendriplexes system (Fig. 2 B&C), while the cross-section (height measurement) of single lipodendriplex also depicted the results according to the hydrodynamic size obtained by DLS analysis (Fig. 2 D). Fig. 2 D also showed a step height of 4 nm representing the presence of lipid bilayer on the particle.

3.2. Reactive oxygen species (ROS) generation

It has been reported that toxicity produced by exposed terminal amino groups of PAMAM dendrimer played a crucial role in ROS generation, which is directly associated with mitochondrial membrane permeabilization and disruption of mitochondrial transduction pathways (Naha et al., 2010). In our study, we have used H_2DCFDA (a fluorogenic dye) for the detection of ROS generation in Caco-2 cells. After permeation into the cells, H_2DCFDA was enzymatically deacetylates by cellular esterase to H_2DCF (a non-fluorescent compound) that was further oxidized to DCF (green fluorescent) by intracellular ROS (Szychowski et al., 2016). The results of ROS generation showed that the cells incubated with dendriplexes produce significantly higher DCF signals as compared to lipodendriplexes, indicating the shield of liposome against PAMAM dendrimer induced toxicity. The microscopic evaluation showing the lower green fluorescent signals by lipodendriplexes system further confirming the role of the exposed terminal amino group in ROS production (Fig. 2 E&F).

3.3. In vitro cell viability (MTT assay)

In vitro cell viability studies, using MTT assay were carried out in Caco-2 cell line to check the toxicity associated with the optimized complexes. It has been reported that dendriplexes having polycationic terminal amino groups exhibited cytotoxicity due to their interaction with the oppositely charged surface of cellular membranes and lead to

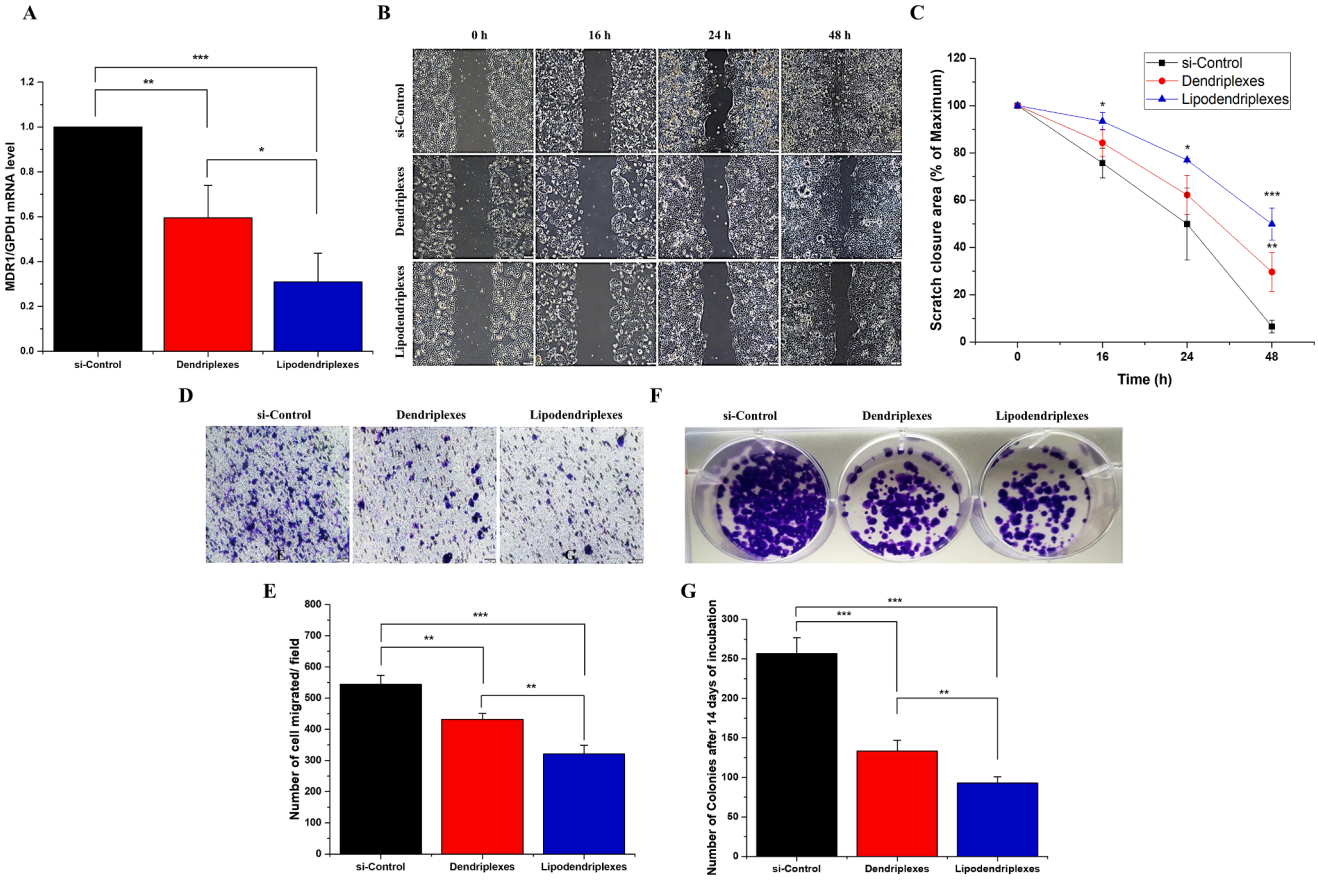

Fig. 3. (A) RT-qPCR analysis for *MDR1* gene silencing. (B) Scratch closure assay; microscopic evaluation up to 48 h. Scale bar represents 100 μm. (C) Graphical presentation of scratch closure area over the time period of 48 h i.e. the percentage of maximum area at 0 h. (D) Transwell cell migration assay using phase-contrast microscopy of the cells stained with 0.1% crystal violet. Scale bar represents 20 μm. (E) Graphical representation of the number of cells migrated per field. (F) Colony formation assay; Photographs of the cells colony stained with 0.1% crystal violet. (G) Graphical presentation of the number of colony formation after 14 days of incubation in Caco-2 cell line of optimized dendriplexes and of DPPC: CH-PAMAM lipodendriplexes (N/P ratio 12). Cells treated with non-specific scrambled siRNA considered as si-Control. Values are represented as mean ± S.D (n = 3) and statistical significances are indicated as *$p < 0.05$, **$p < 0.01$, ***$p < 0.001$. (For interpretation of the references to color in this figure legend, the reader is referred to the web version of this article.)

their structural disruptions (Movassaghian et al., 2011). As shown in Fig. 2 G, the dendriplexes treated cells showed less viability (i.e. 76.4 ± 6.4%) in comparison to lipodendriplexes and si-Control treated cells (i.e. 98.2 ± 14.5% and 100.2 ± 27.3%, respectively).

3.4. Lysosomal disruption and actin polymerization

For an efficient nucleic acid delivery, the cargo should be stable during the endocytic uptake to release into the cytosol (Nguyen et al., 2008). It has been reported that endocytosis is the main mechanism of cellular uptake of protonated PAMAM dendrimers which trafficked to lysosomes to buffered the endolysosomal pH (proton sponge effect) and can lead lysosomal rupturing by lysosomal membrane permeabilization (LMP) mechanism (Kitchens et al., 2007; Thomas et al., 2009). Cell death associated with LMP is highly associated with mitochondrial membrane permeabilization that can result in enhanced reactive oxygen species (ROS) generation, cytosolic acidification and cellular necrosis (Stern et al., 2012). It has also been reported that the PAMAM dendrimer can interact with the cytoskeleton in a biphasic manner. At low concentrations, they retard the actin polymerization by acting as G-binding actin protein while at higher concentrations they behave as a nucleating protein to cause actin polymerization (Ruenraroengsak and Florence, 2010; Shen et al., 2018). Therefore, to investigate the intracellular trafficking of PAMAM based complexes, LysoTracker® red DND-99 (lysosomal marker) and Phalloidin FITC (cytoskeleton staining dye) were used. Fig. 2 H depicted that after the incubation period of 4 h, the cells treated with lipodendriplexes showed a higher fluorescence intensity of Lysotracker red as compared to dendriplexes suggesting a lower damaging and of lysosomes by the lipid-modified system. It was further observed that the concentration of PAMAM dendrimer used in the complexes does not alter the structure of the cytoskeleton and inhibit the actin polymerization process.

3.5. DNA damage assay

It has been evaluated from the above sections; the naked dendriplexes were responsible for enhanced oxidative stress and mitochondrial membrane permeabilization that are the key determinants of cellular toxicity. The free radical formation was further responsible for the damage of many biological components including cellular proteins and DNA, which may lead to apoptosis and cellular necrosis (Naha and Byrne, 2013). The alkaline comet assay also called a single cell gel electrophoresis method, is a fast and reliable method for the determination of DNA damage. If there is some damage or fragments present in a negatively charged DNA, the broken part may migrate towards the anode to resolve into DNA head and tail, similar to a broken comet. From the results, it was assessed that the lipodendriplexes exhibited less DNA damage with an olive tail moment of 0.7 ± 1.0 while in the case of dendriplexes it was significantly ($p < 0.01$) high i.e. 7.6 ± 4.4 (Fig. 2 I&J).

Hence, the exposed terminal amino groups on the surface of naked dendriplexes were considered responsible for ROS generation,

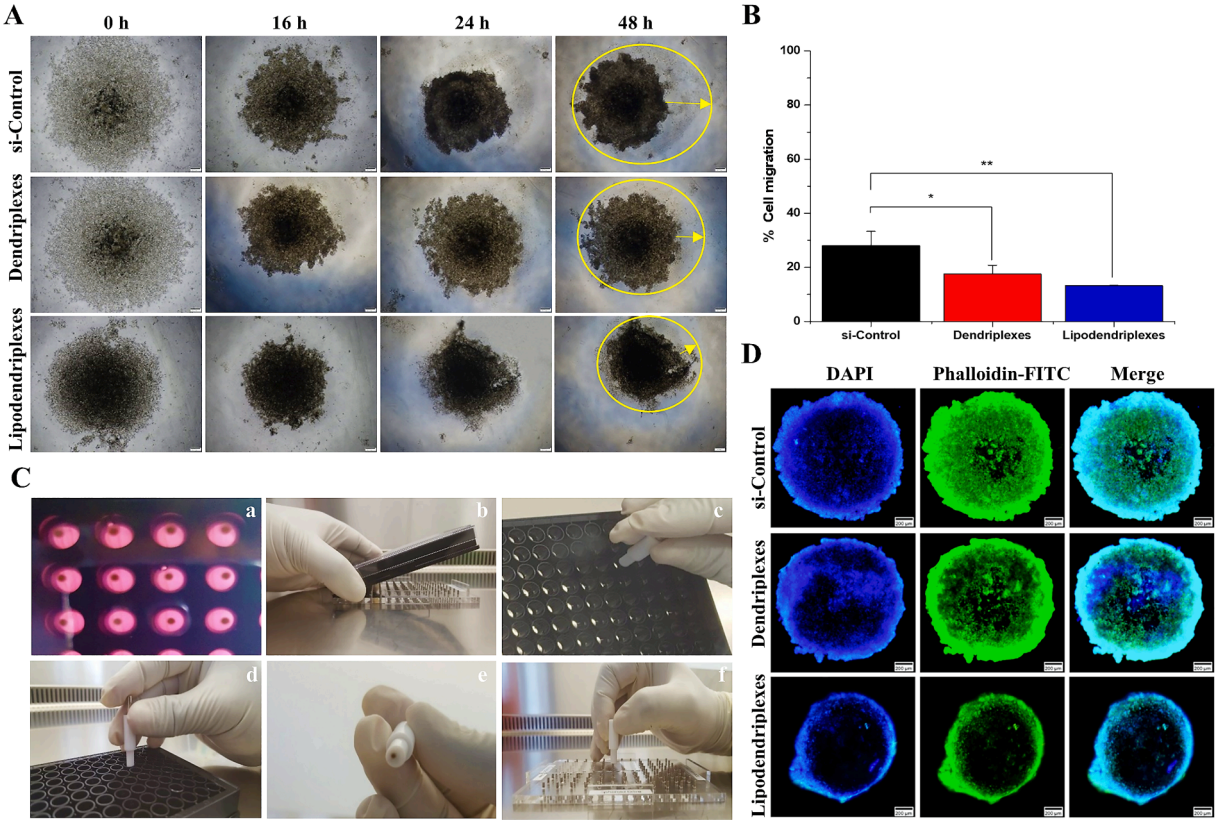

Fig. 4. (A) 3D tumor spheroid cell migration assay in Caco-2 cell line of optimized dendriplexes and of DPPC: CH-PAMAM lipodendriplexes (N/P ratio 12). (B) Graphical representation of the percentage of cell migration from the original bioprinted area after 48 h. (C) Steps involved in staining and transferring the 3D tumor spheroid on the glass slides (a) Overview of spheroids in 96-well ultra-low attachment plate. (b) Placement of plate on a spheroid magnetic drive to hold the spheroids during washing, fixing and staining. (c) Move the Magpen to a well of 96-well plate to pick up a spheroid. (d) Removal of Magpen out of well (a magnet will stay on the pen). (e) A typical spheroid is attached to the underside of the pen. (f) Place the pen (without magnet) on the glass slide to place the spheroid, under the influence of the magnetic field. (D) Cytoskeleton staining of spheroids. DAPI (blue) corresponds to the nuclei staining while Phalloidin FITC (green) representing the cytoskeleton staining to monitor actin polymerization. Cells treated with non-specific scrambled siRNA were used as si-Control. Scale bar represents 200 μm. Values are represented as mean ± S.D (n = 3) and statistical significances are indicated as *$p < 0.05$, **$p < 0.01$. (For interpretation of the references to color in this figure legend, the reader is referred to the web version of this article.)

mitochondrial damage, cytotoxicity and DNA damage.

3.6. RNA interference experiments

3.6.1. MDR1 gene silencing

The RT-qPCR assay was performed to measure the gene silencing mediated by si-*MDR*1 complexes. It was observed that lipid-modified complexes exhibited 70% *MDR1* gene silencing ($p < 0.001$) which was 1.7 higher than naked dendriplexes ($p < 0.01$) i.e. 41% knockdown, as shown in Fig. 3 A.

3.6.2. Wound healing assay

P-glycoproteins (P-gp), encoded by the *MDR1* gene, are not only involved in the drug efflux mechanism, but they can also play a major role in the promotion of tumor metastasis and provide protection of tumor cells against caspase-dependent apoptosis (Katoh et al., 2008; Zhang et al., 2014). To investigate the role of *MDR1* gene in tumor metastasis, Caco-2 cells were transfected with si-*MDR1* complexes and tumor progression was evaluated by wound healing assay, using Ibidi culture inserts. It was observed that the knockdown of *MDR1* gene by lipodendriplexes exhibited less scratch closure as compared to dendriplexes and si-Control groups (Fig. 3 B). Results showed that in comparison to si-Control, the percentage of the scratch closure in lipodendriplexes and dendriplexes treated cells were 23% ($p < 0.001$) and 47% ($p < 0.01$), respectively (Fig. 3 C). Therefore, it is evident from the findings, the enhanced downregulation of *MDR1* by lipodendriplexes contributes to inhibition of metastatic progression.

3.6.3. Transwell migration assay

Cell migration was further investigated by the transwell migration assay. It has been observed that in comparison to si-Control group, lipodendriplexes treated cells exhibited a significant reduction ($p < 0.001$) in cell migration (approximately 41% decreased) while 20% reduction ($p < 0.01$) was observed in the case of dendriplexes treated cells (Fig. 3 D&E). Hence, the results of transwell migration assay were in good correlation with the results obtained in scratch closure assay.

3.6.4. Plate colony formation assay

Downregulation of *MDR1* is also responsible for the suppression of cell proliferation and colonization (Katoh et al., 2008). To confirm this role of *MDR1* in colon cancer, colony formation assay was performed in Caco-2 cell line. It was observed that after knockdown of *MDR1* gene with lipodendriplexes, the number of colony formation was significantly ($p < 0.001$) reduced to 63%, compared to the si-Control group. Similar effects were recorded in dendriplexes treated group with an inhibition effect of about 48% ($p < 0.001$). Nevertheless, the knockdown produced by lipodendriplexes exhibited more significant ($p < 0.01$) results as compared to the parent dendriplexes group (Fig. 3 F&G). These results depicted that *MDR1* knockdown played an obvious role in the inhibition of cell proliferation and colonization of Caco-2 cells.

3.7. 3D tumor spheroid cell migration assay

Cell migration plays a vital role in tumor metastasis. Therefore, to investigate the cell metastasis in Caco-2 cells, magnetically levitated cells were patterned into a 3D tumor spheroidal model to establish a similar *in vivo* tumor-like environment (Wiercinska et al., 2011). This 3D tumor model determines the impact of *MDR1* silencing on tumor progression. The cells treated with complexes containing si-*MDR1* were allowed to migrate through ECM (away from the original bioprinted

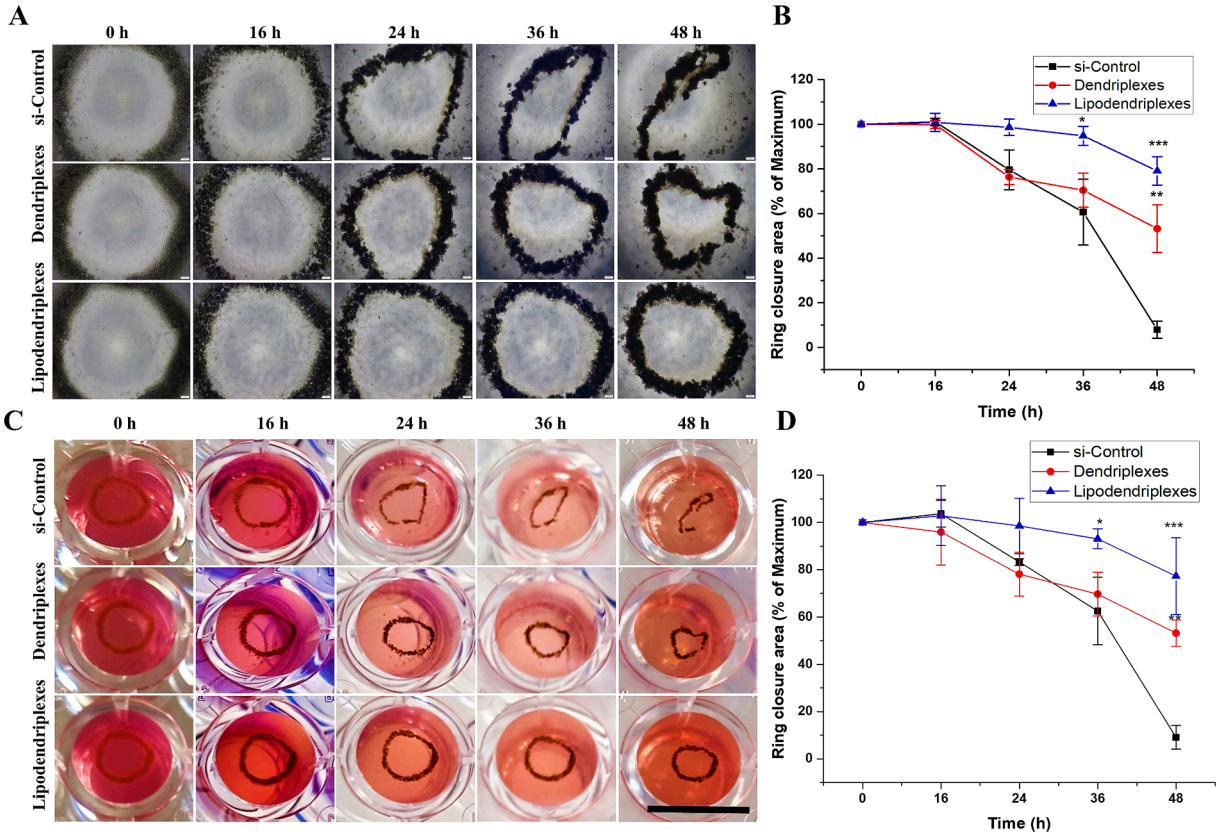

Fig. 5. 3D tumor ring closure assay using (A) a phase-contrast microscope and by (C) a mobile device while (B&D) depicting their graphical representation respectively, in Caco-2 cell line of optimized dendriplexes and DPPC: CH-PAMAM lipodendriplexes (N/P ratio 12) at specified time (h) intervals. Cells treated with non-specific scrambled siRNA considered as si-Control. White scale bar represents 200 μm. Black scale bar represents 5 mm. Values are represented as mean ± S.D (n = 3) and statistical significances are indicated as *$p < 0.05$, **$p < 0.01$, ***$p < 0.001$.

area) and the percentage of cell migration over the incubation period of 48 h was recorded. The results showed that in the case of si-Control treated cells the percentage of cell migration was 28% while a significant reduction in cell migration was found in the case of dendriplexes ($p < 0.05$) and lipodendriplexes ($p < 0.01$) treated groups i.e. 18% and 13%, respectively (Fig. 4 A&B).

3.8. Cytoskeleton staining of spheroids

It is difficult to handle the spheroids during the staining process. Therefore, in the case of a magnetically printed spheroid, for every step including washing, fixing and staining, the magnetic drive was placed under the plate to maintain the integrity of the spheroids. The Magpen was used to lift the stained spheroid and to place them on the slide for analysis (Fig. 4 C). The visualization of actin, in 2D culture of Caco-2 cells, was analysed in Section 3.4 to investigate the process of actin polymerization. Similarly, the staining of actin was conducted in 3D culture to observe the distribution of cytoskeleton, which are responsible for cell-matrix adhesion and shape of the spheroids. Fig. 4 D illustrated that the spheroids treated with si-Control showed a loose cellular distribution due to their ability to migrate in outer media while in the case of lipodendriplexes treated cells, the intracellular layer was strongly adhered to the extracellular matrix and anchored the spheroids, responsible for the reduction in cell migration.

3.9. 3D tumor ring closure assay using phase-contrast microscopy

Ring closure assay is similar to a scratch closure assay (2D culture) in which the void circular space tends to close in 3D fashion over a specific time period (Tseng et al., 2015). Ring closure assay was performed on the magnetically levitated cells to investigate the role of *MDR1* gene in cell migration using 3D bioprinted cells. The cells treated with complexes containing si-*MDR1* were patterned into 3D ring structure and the ring closure was recorded for 48 h to evaluate the gene silencing effect.

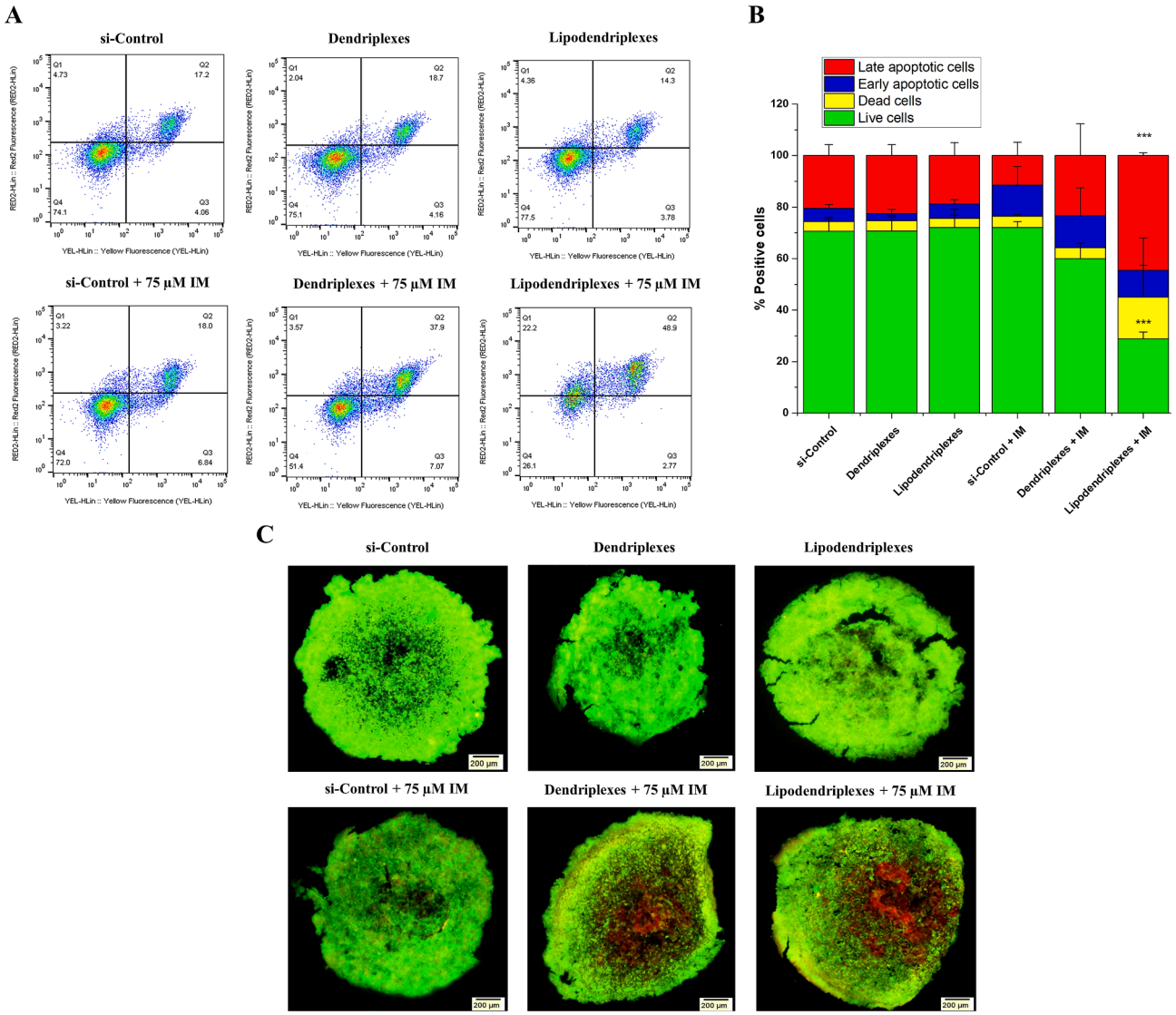

Fig. 6. Apoptosis assay in Caco-2 cell line using optimized dendriplexes and of DPPC: CH-PAMAM lipodendriplexes (N/P ratio 12) without or with (75 µM) IM treatment. (A) FACS micrographs indicating; Left bottom = healthy cells, right bottom = dead cells, left top = early apoptotic cells, right top = late apoptotic cells. (B) Graphical representation of percentage (%) of positive cells. Green, yellow, blue and red bar graphs representing live, dead, early apoptotic and late apoptotic cells, respectively. (C) Live dead staining of spheroids for apoptosis determination by fluorescence microscopy. Green fluorescence (syto 9) representing the live cells while red fluorescence (PI) indicating dead and late apoptotic cells. Cells treated with non-specific scrambled siRNA considered as control. Scale bar represents 200 µm. Values are represented as mean ± S.D (n = 3) and statistical significances are indicated as *$p < 0.05$, ***$p < 0.001$. (For interpretation of the references to color in this figure legend, the reader is referred to the web version of this article.)

The percentage of ring closure was determined by measuring the inner diameter of the ring at specific time intervals (0, 16, 24, 36, 48 h). The results of Fig. 5 A showed that the cells treated with lipodendriplexes slower the ring closure as compared to dendriplexes and si-Control treated cells. After 48 h incubation, the cells treated with si-Control shrink the ring to 92% while in comparison to si-Control, a significant reduction in ring closure was found in the case of dendriplexes ($p < 0.01$) and lipodendriplexes ($p < 0.001$) with a reduction in the inner diameter of 47% and 21%, respectively (Fig. 5 B).

3.10. 3D tumor ring closure assay using mobile device

Ring closure area was also determined by a less expensive mobile device in comparison to the phase-contrast imaging microscope. The dark brown colouration of the ring makes it possible to capture the change in diameter in individual well on a microtiter plate (Fig. 5 C). It was observed that the results obtained using a mobile device were similar to the phase-contrast microscope, but the lower resolution power did not provide the exact results. About 91% of ring closure was recorded in si-Control treated cells while 45% ($p < 0.01$) and 23% ($p < 0.001$) were observed in the case of dendriplexes and lipodendriplexes, respectively (Fig. 5D).

3.11. Apoptosis assay by flow cytometry

Sequential treatment of RNA interference and chemotherapy provides a synergistic effect to resolve the issue of multidrug resistance (Liu et al., 2017). The overexpression of P-gp on Caco-2 cells are responsible for the efflux of imatinib mesylate (IM). Therefore, the effective downregulation of P-gp can enhance the intracellular accumulation of the IM and subsequent apoptosis of the cells. To investigate the apoptosis by flow cytometry (FACS), one group of the cells were incubated with si-Control, dendriplexes, lipodendriplexes and the other group of the cells were subjected to a sequential treatment of si-Control, dendriplexes, lipodendriplexes followed by 75 μM of IM. It has been observed that the downregulation of P-gp was accountable for the increased apoptosis of the cells (Fig. 6 A). The results of Fig. 6 B showed that the cells which were only incubated with si-Control, dendriplexes and lipodendriplexes exhibited 23.5 ± 5.5%, 25.3 ± 5.7% and 24.4 ± 6.7% cellular apoptosis (early + late apoptosis), respectively. Contrarily, a sequential treatment increased the subsequent cellular apoptosis. It has been observed that the lipodendriplexes aided sequential treatment significantly increased the apoptosis (54.9 ± 13.7%) in comparison to dendriplexes ($p < 0.05$) and si-Control group ($p < 0.001$) i.e. 35.7 ± 23.1% and 24.5 ± 12.3% respectively. Therefore, the downregulation of P-gp with the help of lipodendriplexes was responsible for the re-sensitization of the cells for enhanced intracellular accumulation of drug (IM).

3.12. Apoptosis determination of spheroids by live dead viability assay

In contrast to 2D culture, the live dead viability assay was performed in 3D tumor spheroidal model for apoptosis investigation. The live cells were stained with syto 9 while dead and late apoptotic cells were stained with PI. For the apoptotic determination, the equilibrated spheroids of si-Control, dendriplexes and lipodendriplexes were incubated without or with IM (75 μM) treatment for 24 h. The spheroids only incubated with si-Control, dendriplexes and lipodendriplexes maintain their cellular integrity and showed a dense outer layer of live cells, with a small portion of dead cells, while the IM treated spheroids exhibited a change in shape depicted a hollow cellular structure, indicating the loss of cell fragments from the spheroids. Results of Fig. 6 C showed that after the IM treatment, the lipodendriplexes treated cells exhibited maximum apoptotic effects and showed an enhanced red fluorescence of PI channel in spheroidal structure as compared to dendriplexes and si-Control treated group. These results further confirmed the enhanced intracellular accumulation of IM following the efficient knockdown by lipodendriplexes system and were in good correlation with the results obtained from apoptosis assay in 2D culture.

3.13. Cell cycle analysis and accumulation of Sub-G1 phase

The cell cycle analysis was performed to determine the cell phase distribution by flow cytometry analysis. Results of Fig. 7 A depicted the effective downregulation of P-gp expression contributes to the apoptosis induced by IM and arrests the cell cycle at Sub-G1 phase. Fig. 7 B showed

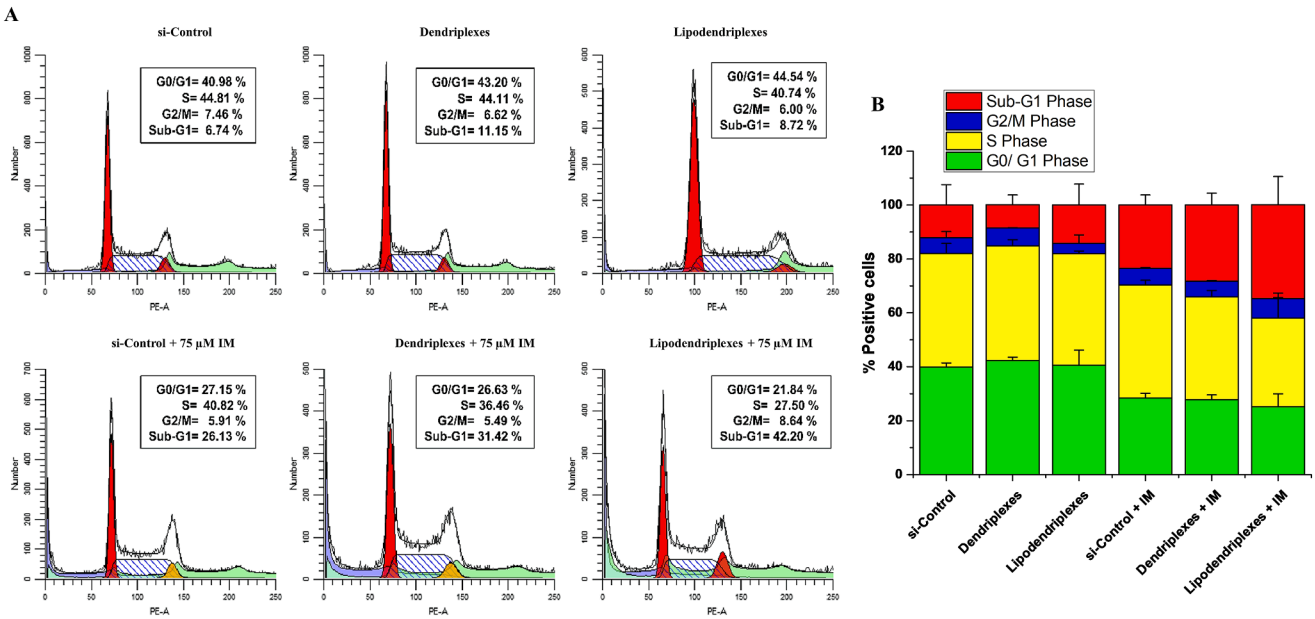

Fig. 7. Cell cycle analysis by flow cytometry in Caco-2 cell line by optimized dendriplexes and of DPPC: CH-PAMAM lipodendriplexes (N/P ratio 12) without or with IM treatment (75 μM). (A) FACS micrographs and (B) graphical representation of percentage (%) of positive cells. Green, yellow, blue and red bar graphs representing G0/G1, S, G2/ M and Sub-G1 phases, respectively. Cells treated with non-specific scrambled siRNA considered as si-Control. Values are represented as mean ± S.D (n = 2). (For interpretation of the references to color in this figure legend, the reader is referred to the web version of this article.)

that the cells incubated with si-Control, dendriplexes and lipodendriplexes exhibited 12.0 ± 5.5%, 8.6 ± 3.5% and 14.2 ± 7.7% of Sub-G1 phase distribution. While an increased percentage in Sub-G1 phase was observed after the sequential treatment, depicting an increased Sub-G1 phase with lipodendriplexes treated group (34.7 ± 10.3%) in comparison to dendriplexes (28.2 ± 4.4%) and si-Control groups (23.4 ± 3.7%). These findings suggest that enhanced intracellular accumulation of IM arrests the Caco-2 cell cycle at the Sub-G1 phase.

4. Conclusion

From the current study, it is evident that the lipodendriplexes system is a safe and efficient nanocarrier for siRNA delivery in colon carcinoma. Cytotoxicity studies including, ROS, *in vitro* cell viability, lysosomal disruption and DNA damage assay revealed that the lipid modification of dendriplexes significantly shields the terminal amino group induced toxicity and consequently improves the cell viability. The RNA interference experiments in 2D and 3D environments also witnessed the pronounced cellular uptake and subsequent downregulation of *MDR1* genes depicted a significant inhibition of tumor metastasis and colonization by such an optimized system. The sequential downregulation of *MDR1* gene and chemotherapy has shown enhanced apoptosis of cancer cells, addressed a novel strategy to overcome the challenges associated with multi-drug resistant cancers. Therefore, this optimized system has the full potential to be used for further *in vivo* studies, by using ligand-specific targeting systems, against different types of cancer.

CRediT authorship contribution statement

Imran Tariq: Conceptualization, Investigation, Writing - original draft, Formal analysis, Visualization. **Muhammad Yasir Ali:** Investigation, Writing - original draft. **Harshavardhan Janga:** Methodology, Investigation. **Sajid Ali:** Investigation, Formal analysis. **Muhammad Umair Amin:** Investigation. **Ghazala Ambreen:** Methodology, Investigation. **Uzma Ali:** Methodology, Investigation. **Shashank Reddy Pinnapireddy:** Writing - review & editing, Validation, Investigation. **Jens Schäfer:** Validation, Conceptualization, Writing - review & editing. **Leon N. Schulte:** Validation, Investigation, Writing - review & editing. **Udo Bakowsky:** Project administration, Supervision, Resources, Conceptualization, Writing - review & editing.

Declaration of Competing Interest

The authors declare that they have no known competing financial interests or personal relationships that could have appeared to influence the work reported in this paper.

Acknowledgment

The authors would like to thank the Overseas Scholarship Committee of University of the Punjab, Higher Education Commission (HEC) of Pakistan and German Academic Exchange Service (DAAD) for providing scholarship grants. The authors extend their gratitude to Mrs. Eva Mohr for her technical support in cell culture experiments.

Appendix A. Supplementary material

Supplementary data to this article can be found online at https://doi.org/10.1016/j.ijpharm.2020.119993.

References

Ali, S., Amin, M.U., Ali, M.Y., Tariq, I., Pinnapireddy, S.R., Duse, L., Goergen, N., Wölk, C., Hause, G., Jedelská, J., 2020. Wavelength dependent photo-cytotoxicity to ovarian carcinoma cells using temoporfin loaded tetraether liposomes as efficient drug delivery system. Eur. J. Pharm. Biopharm. 150, 5–65.

Balachandran, V.P., Cavnar, M.J., Zeng, S., Bamboat, Z.M., Ocuin, L.M., Obaid, H., Sorenson, E.C., Popow, R., Ariyan, C., Rossi, F., 2011. Imatinib potentiates antitumor T cell responses in gastrointestinal stromal tumor through the inhibition of Ido. Nat. Med. 17 (9), 1094–1100.

Biswas, S., Deshpande, P.P., Navarro, G., Dodwadkar, N.S., Torchilin, V.P., 2013. Lipid modified triblock PAMAM-based nanocarriers for siRNA drug co-delivery. Biomaterials 34 (4), 1289–1301.

Dantzig, A.H., de Alwis, D.P., Burgess, M., 2003. Considerations in the design and development of transport inhibitors as adjuncts to drug therapy. Adv. Drug Deliv. Rev. 55 (1), 133–150.

de Cássia Antonino, D., Soares, M.M., de Melo Júnior, J., de Alvarenga, P.B., Mohallem, R.D.F.F., Rocha, C.D., Vieira, L.A., de Souza, A.G., Beletti, M.E., Alves, B. G., 2019. Three-dimensional levitation culture improves in-vitro growth of secondary follicles in bovine model. Reprod. Biomed. online 38 (3), 300–311.

Druker, B.J., Sawyers, C.L., Kantarjian, H., Resta, D.J., Reese, S.F., Ford, J.M., Capdeville, R., Talpaz, M., 2001. Activity of a specific inhibitor of the BCR-ABL tyrosine kinase in the blast crisis of chronic myeloid leukemia and acute lymphoblastic leukemia with the Philadelphia chromosome. N. Engl. J. Med. 344 (14), 1038–1042.

Duse, L., Pinnapireddy, S.R., Strehlow, B., Jedelská, J., Bakowsky, U., 2018. Low level LED photodynamic therapy using curcumin loaded tetraether liposomes. Eur. J. Pharm. Biopharm. 126, 233–241.

Dutta, T., Aghase, H.B., Vijayarajkumar, P., Joshi, M., Jain, N., 2006. Dendrosome-based gene delivery. J. Exp. Nanosci. 1 (2), 235–248.

Dutta, T., Burgess, M., McMillan, N.A., Parekh, H.S., 2010. Dendrosome-based delivery of siRNA against E6 and E7 oncogenes in cervical cancer. Nanomed. Nanotechnol. Biol. Med. 6 (3), 463–470.

Essex, S., Navarro, G., Sabhachandani, P., Chordia, A., Trivedi, M., Movassaghian, S., Torchilin, V.P., 2014. Phospholipid-modified PEI-based nanocarriers for in vivo siRNA therapeutics against multidrug-resistant tumors. Gene Ther. 22, 257–266.

Galimberti, S., Cervetti, G., Guerrini, F., Testi, R., Pacini, S., Fazzi, R., Simi, P., Petrini, M., 2005. Quantitative molecular monitoring of BCR-ABL and MDR1 transcripts in patients with chronic myeloid leukemia during Imatinib treatment. Cancer Genet. Cytogenet. 162 (1), 57–62.

Gilleron, J., Querbes, W., Zeigerer, A., Borodovsky, A., Marsico, G., Schubert, U., Manygoats, K., Seifert, S., Andree, C., Stöter, M., 2013. Image-based analysis of lipid nanoparticle–mediated siRNA delivery, intracellular trafficking and endosomal escape. Nat. Biotechnol. 31 (7), 638–646.

Graber-Maier, A., Gutmann, H., Drewe, J., 2010. A new intestinal cell culture model to discriminate the relative contribution of P-gp and BCRP on transport of substrates such as imatinib. Mol. Pharm. 7 (5), 1618–1628.

Guo, N., Gao, C., Liu, J., Li, J., Liu, N., Hao, Y., Chen, L., Zhang, X., 2018. Reversal of ovarian cancer multidrug resistance by a combination of LAH4-L1-siMDR1 nanocomplexes with chemotherapeutics. Mol. Pharm. 15 (5), 1853–1861.

Iqbal, N., Iqbal, N., 2014. Imatinib: a breakthrough of targeted therapy in cancer. Chemother. Res. Pract. 2014.

Jain, K., Kesharwani, P., Gupta, U., Jain, N., 2010. Dendrimer toxicity: let's meet the challenge. Int. J. Pharm. 394 (1–2), 122–142.

Jiang, J., Yang, S.-J., Wang, J.-C., Yang, L.-J., Xu, Z.-Z., Yang, T., Liu, X.-Y., Zhang, Q., 2010. Sequential treatment of drug-resistant tumors with RGD-modified liposomes containing siRNA or doxorubicin. Eur. J. Pharm. Biopharm. 76 (2), 170–178.

Katoh, S.-Y., Ueno, M., Takakura, N., 2008. Involvement of MDR1 function in proliferation of tumour cells. J. Biochem. 143 (4), 517–524.

Kitchens, K.M., Foraker, A.B., Kolhatkar, R.B., Swaan, P.W., Ghandehari, H., 2007. Endocytosis and interaction of poly (amidoamine) dendrimers with Caco-2 cells. Pharm. Res. 24 (11), 2138–2145.

Liu, J., Li, J., Liu, N., Guo, N., Gao, C., Hao, Y., Chen, L., Zhang, X., 2017. In vitro studies of phospholipid-modified PAMAM-siMDR1 complexes for the reversal of multidrug resistance in human breast cancer cells. Int. J. Pharm. 530 (1–2), 291–299.

MacDiarmid, J.A., Amaro-Mugridge, N.B., Madrid-Weiss, J., Sedliarou, I., Wetzel, S., Kochar, K., Brahmbhatt, V.N., Phillips, L., Pattison, S.T., Petti, C., 2009. Sequential treatment of drug-resistant tumors with targeted minicells containing siRNA or a cytotoxic drug. Nat. Biotechnol. 27 (7), 643–651.

Mahmoud, G., Jedelská, J., Omar, S.M., Strehlow, B., Schneider, M., Bakowsky, U., 2018. Stabilized tetraether lipids based particles guided prophyrins photodynamic therapy. Drug Delivery 25 (1), 1526–1536.

Mahon, F.-X., Belloc, F., Lagarde, V., Chollet, C., Moreau-Gaudry, F., Reiffers, J., Goldman, J.M., Melo, J.V., 2003. MDR1 gene overexpression confers resistance to imatinib mesylate in leukemia cell line models. Blood 101 (6), 2368–2373.

Movassaghian, S., Moghimi, H.R., Shirazi, F.H., Torchilin, V.P., 2011. Dendrosome-dendriplex inside liposomes: as a gene delivery system. J. Drug Target. 19 (10), 925–932.

Naha, P.C., Byrne, H.J., 2013. Generation of intracellular reactive oxygen species and genotoxicity effect to exposure of nanosized polyamidoamine (PAMAM) dendrimers in PLHC-1 cells in vitro. Aquat. Toxicol. 132, 61–72.

Naha, P.C., Davoren, M., Lyng, F.M., Byrne, H.J., 2010. Reactive oxygen species (ROS) induced cytokine production and cytotoxicity of PAMAM dendrimers in J774A. 1 cells. Toxicol. Appl. Pharmacol. 246 (1–2), 91–99.

Negi, L.M., Jaggi, M., Joshi, V., Ronodip, K., Talegaonkar, S., 2015. Hyaluronan coated liposomes as the intravenous platform for delivery of imatinib mesylate in MDR colon cancer. Int. J. Biol. Macromol. 73, 222–235.

Nguyen, J., Steele, T.W., Merkel, O., Reul, R., Kissel, T., 2008. Fast degrading polyesters as siRNA nano-carriers for pulmonary gene therapy. J. Control. Release 132 (3), 243–251.

Ni, L.-N., Li, J.-Y., Miao, K.-R., Qiao, C., Zhang, S.-J., Qiu, H.-R., Qian, S.-X., 2011. Multidrug resistance gene (MDR1) polymorphisms correlate with imatinib response in chronic myeloid leukemia. Med. Oncol. 28 (1), 265–269.
Risnayanti, C., Jang, Y.-S., Lee, J., Ahn, H.J., 2018. PLGA nanoparticles co-delivering MDR1 and BCL2 siRNA for overcoming resistance of paclitaxel and cisplatin in recurrent or advanced ovarian cancer. Sci. Rep. 8 (1), 1–12.
Ruenraroengsak, P., Florence, A.T., 2010. Biphasic interactions between a cationic dendrimer and actin. J. Drug Target. 18 (10), 803–811.
Sarisozen, C., Pan, J., Dutta, I., Torchilin, V.P., 2017. Polymers in the co-delivery of siRNA and anticancer drugs to treat multidrug-resistant tumors. J. Pharm. Invest. 47 (1), 37–49.
Saw, P.E., Park, J., Jon, S., Farokhzad, O.C., 2017. A drug-delivery strategy for overcoming drug resistance in breast cancer through targeting of oncofetal fibronectin. Nanomed. Nanotechnol. Biol. Med. 13 (2), 713–722.
Shen, Z.-L., Tian, W.-D., Chen, K., Ma, Y.-Q., 2018. Molecular dynamics simulation of G-actin interacting with PAMAM dendrimers. J. Mol. Graph. Model. 84, 145–151.
Stern, S.T., Adiseshaiah, P.P., Crist, R.M., 2012. Autophagy and lysosomal dysfunction as emerging mechanisms of nanomaterial toxicity. Part. Fibre Toxicol. 9 (1), 20.
Stromskaya, T., Rybalkina, E.Y., Kruglov, S., Zabotina, T., Mechetner, E., Turkina, A., Stavrovskaya, A., 2008. Role of P-glycoprotein in evolution of populations of chronic myeloid leukemia cells treated with imatinib. Biochemistry (Moscow) 73 (1), 29–37.
Szychowski, K.A., Rybczyńska-Tkaczyk, K., Leja, M.L., Wójtowicz, A.K., Gmiński, J., 2016. Tetrabromobisphenol A (TBBPA)-stimulated reactive oxygen species (ROS) production in cell-free model using the 2′, 7′-dichlorodihydrofluorescein diacetate (H 2 DCFDA) assay—limitations of method. Environ. Sci. Pollut. Res. 23 (12), 12246–12252.
Tariq, I., Pinnapireddy, S.R., Duse, L., Ali, M.Y., Ali, S., Amin, M.U., Goergen, N., Jedelská, J., Schäfer, J., Bakowsky, U., 2019. Lipodendriplexes: a promising nanocarrier for enhanced gene delivery with minimal cytotoxicity. Eur. J. Pharm. Biopharm. 135, 72–82.
Terashima, J., Sampei, S., Iidzuka, M., Ohsakama, A., Tachikawa, C., Satoh, J., Kudo, K., Habano, W., Ozawa, S., 2016. VEGF expression is regulated by HIF-1α and ARNT in 3D KYSE-70, esophageal cancer cell spheroids. Cell Biol. Int. 40 (11), 1187–1194.
Thomas, T.P., Majoros, I., Kotlyar, A., Mullen, D., Banaszak Holl, M.M., Baker, J.R., 2009. Cationic poly(amidoamine) dendrimer induces lysosomal apoptotic pathway at therapeutically relevant concentrations. Biomacromolecules 10 (12), 3207–3214.
Timm, D.M., Chen, J., Sing, D., Gage, J.A., Haisler, W.L., Neeley, S.K., Raphael, R.M., Dehghani, M., Rosenblatt, K.P., Killian, T., 2013. A high-throughput three-dimensional cell migration assay for toxicity screening with mobile device-based macroscopic image analysis. Sci. Rep. 3, 1–8.
Tseng, H., Gage, J.A., Haisler, W.L., Neeley, S.K., Shen, T., Hebel, C., Barthlow, H.G., Wagoner, M., Souza, G.R., 2016. A high-throughput in vitro ring assay for vasoactivity using magnetic 3D bioprinting. Sci. Rep. 6, 1–8.
Tseng, H., Gage, J.A., Shen, T., Haisler, W.L., Neeley, S.K., Shiao, S., Chen, J., Desai, P.K., Liao, A., Hebel, C., 2015. A spheroid toxicity assay using magnetic 3D bioprinting and real-time mobile device-based imaging. Sci. Rep. 5, 1–11.
Tsuruo, T., Naito, M., Tomida, A., Fujita, N., Mashima, T., Sakamoto, H., Haga, N., 2003. Molecular targeting therapy of cancer: drug resistance, apoptosis and survival signal. Cancer Sci. 94 (1), 15–21.
Wiercinska, E., Naber, H.P., Pardali, E., van der Pluijm, G., van Dam, H., Ten Dijke, P., 2011. The TGF-β/Smad pathway induces breast cancer cell invasion through the up-regulation of matrix metalloproteinase 2 and 9 in a spheroid invasion model system. Breast Cancer Res. Treat. 128 (3), 657–666.
Zhang, F., Zhang, H., Wang, Z., Yu, M., Tian, R., Ji, W., Yang, Y., Niu, R., 2014. P-glycoprotein associates with Anxa2 and promotes invasion in multidrug resistant breast cancer cells. Biochem. Pharmacol. 87 (2), 292–302.
Zhou, J., Wu, J., Hafdi, N., Behr, J.-P., Erbacher, P., Peng, L., 2006. PAMAM dendrimers for efficient siRNA delivery and potent gene silencing. Chem. Commun. (22), 2362–2364.